

pubs.acs.org/cm Article

In Situ Evolution of Ru₄Al₁₃ Crystals into a Highly Active Catalyst for the Hydrogen Evolution Reaction

Kriti Seth, Albert J. Darling, Cameron F. Holder, Yihuang Xiong, Jeffrey R. Shallenberger, and Raymond E. Schaak*



Cite This: Chem. Mater. 2021, 33, 7124-7131



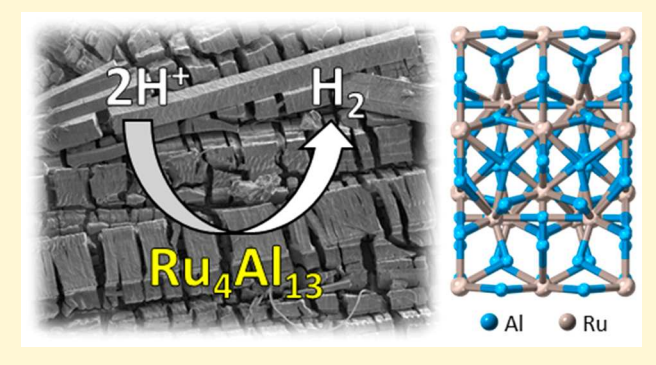
ACCESS

III Metrics & More

Article Recommendations

Supporting Information

ABSTRACT: Materials that catalyze the hydrogen evolution reaction (HER) are important for producing H₂ as a zero-emission fuel. Ru-based materials are becoming increasingly studied as HER catalysts because they often perform comparably to Pt, the benchmark for this reaction. Despite the availability of a growing number of high surface area Ru-based HER catalysts, these materials can be challenging to synthesize. In contrast, bulk Ru-based materials can be readily synthesized by using established solid-state chemistry techniques. While bulk compounds are undesirable as practical catalysts because of their low surface areas, they allow candidate catalysts that are not yet accessible as high surface area materials to be evaluated and studied. Using this approach for Ru-based materials, we show here that the surfaces of millimeter-scale single



crystals of the intermetallic compound Ru_4Al_{13} become rough, pitted, and enriched in Ru, consistent with computed Pourbaix diagrams, upon exposure to acid due to selective Al leaching. The resulting material, having a Ru-rich Ru-Al surface and a Ru_4Al_{13} core, catalyzes the HER in 0.5 M H_2SO_4 with overpotentials of 18 and 39 mV at current densities of -10 and -100 mA/cm², respectively, when normalized to geometric surface areas. These values are comparable to higher surface area nanoparticle catalysts, including Pt. This *in situ* acid-mediated evolution of a bulk crystal into a surface-roughened derivative demonstrates a pathway for engineering catalytic materials that can be readily made as bulk crystals but not yet as higher surface area nanostructures.

■ INTRODUCTION

Molecular hydrogen (H_2) is a zero-emission fuel that produces only water upon combustion and therefore is a desirable alternative to fossil fuels, the use of which results in substantial emissions of CO₂ into the atmosphere. These carbon emissions are primary contributing factors to environmental issues such as climate change, making the development of sustainable methods of H₂ production an important goal.¹ Most H₂ is generated by using steam reforming of natural gas followed by the water-gas shift reaction.² However, this process is energy-intensive and results in the production of CO₂, facilitating the need for the advancement of alternative methods of H₂ production.³ Water splitting, the process of electrocatalytically converting H2O into the gaseous forms of its constituent elements, is an attractive method for H₂ production because it uses H₂O, an abundant and inexpensive resource, as a chemical feedstock, and it can be coupled with solar cells. It is for this reason that much effort has been put into the development of stable catalytic materials that can carry out these processes efficiently.

For the hydrogen evolution reaction (HER) in acidic electrolytes, where proton-exchange membrane fuel cells are most efficient and there is a high concentration of reducible

protons, precious metals are the most efficient, stable, and widely used catalysts. Platinum is considered to be the benchmark heterogeneous catalyst for the HER as the Pt—H bond strength is optimal to facilitate fast kinetics and low overpotentials for H₂ production. However, the high cost and low terrestrial abundance of Pt have motivated the search for alternatives. Newer classes of materials that were found to catalyze the HER in acidic electrolytes include various transition metal alloys, chalcogenides, carbides, borides, and phosphides, as well as metal- and heteroatom-substituted graphitic materials. While some of these materials offer promising alternatives to Pt, they generally remain inferior for many reasons, including higher overpotentials and/or lower acid stability.

Ruthenium-based materials offer an alternative to Pt and are becoming increasingly studied, 6 especially since the Ru–H

Received: July 26, 2021 Revised: August 3, 2021 Published: August 20, 2021





bond strength is similar to that of Pt-H.8 Most Ru-based catalysts that have been studied for the HER are nanoparticles, which maximize the density and accessibility of exposed catalytic active sites.5 Examples of nanostructured Ru-based HER catalysts that are active and relatively stable in acidic electrolytes include Ru-graphene composites,9 ruthenium phosphide (RuP₂) nanoparticles, ¹⁰ and heterostructures of Ru with other transition metals. ¹¹ Particularly notable is the development of composites containing Ru nanoparticles and N-doped graphene nanosheets, which exhibited excellent HER performance that was on par with that of Pt.8 However, while there is a growing number of Ru-based nanocatalysts for the HER,6 nanostructured Ru-based materials are, in general, much more challenging to prepare than many other precious metals, especially as solution-synthesized nanoparticles, given the relatively low reduction potentials of common ruthenium reagents and the susceptibility of Ru surfaces to oxidize. 12,13 In contrast, bulk crystals of Ru-based materials, including intermetallic alloys of Ru with other metals, are straightforward to synthesize for a wide range of compositions and crystal structures. Bulk materials are generally undesirable as practical catalysts because of their low surface areas, but for Ru-based systems, they are strategic targets for fundamental studies because of the greater diversity of compounds that are synthetically accessible and the ability to study how their materials characteristics evolve.

Bulk Ru-Al intermetallic compounds are particularly attractive targets as they alloy an HER-active metal catalyst (Ru) with a corrosion-susceptible metal (Al) and therefore are capable of evolving in acid to change composition and morphology. The most ubiquitous example of this synthetic strategy, using Al-based alloys, has been through the development of Raney Ni, which is a widely used hydrogenation catalyst synthesized by leaching the Al in Ni-Al alloys under alkaline conditions. 14-16 Raney nickel-based materials have seen use as both catalysts and supports for carrying out water-splitting reactions. 17,18 Al leaching has also been used to transform MoAlB single crystals into MoAl_{1-x}B, which has accessible pores that expose catalytically active basal planes that were buried within the crystal prior to removal of Al. 19 In addition, this Al dealloying strategy has been used to produce "Raney Ru" catalysts, which are typically used for ammonia and methanol synthesis. 20-23 Nanoporous Ru catalysts made through dealloying of sputtered Ru-Al films have also been shown to facilitate the production of hydrogen from the hydrolysis of sodium borohydride or ammonia

Here, we show that millimeter-scale crystals of the intermetallic compound $\mathrm{Ru_4Al_{13}}$ evolve, upon exposure to acid, to produce a highly active catalyst for the HER with an overpotential, normalized to geometric surface area, that is comparable to that of Pt benchmarks. Acid treatment of flux-grown single crystals of $\mathrm{Ru_4Al_{13}}$ produces a rough, pitted, Rurich surface due to leaching of the Al in the surface region. A subsequent electrochemical pretreatment process dissolves more of the Al, forming a Ru-rich surface with a $\mathrm{Ru_4Al_{13}}$ core. These chemical processes transform $\mathrm{Ru_4Al_{13}}$ bulk crystals into an acid-stable catalytic material that is highly active for the HER in acidic electrolytes.

The selection of Ru₄Al₁₃ as a candidate catalyst for the HER was based on several factors, beyond the materials and reactivity considerations noted above. First, Ru–Al intermetallic compounds have shown promising results as hydro-

genation catalysts, including the hydrogenation of butadiene to butene. Second, M_4Al_{13} (M= transition metal) compounds have been shown to be excellent catalysts for hydrogenation reactions, which, similarly to the HER, have mechanisms that involve the reversible binding of hydrogen to the catalyst surface. Third, Al doping has been demonstrated to electronically modulate Ru nanostructures to achieve high catalytic performance for the HER. Fourth, Ru–Al intermetallic compounds are not yet accessible as solution-synthesized nanoparticles, and nanostructuring efforts are anticipated to be challenging to accomplish. We therefore view Ru_4Al_{13} as a model system for developing an acid-leaching pathway for transforming a readily accessible bulk crystal into a derivative surface-roughened material exhibiting high catalytic activity.

EXPERIMENTAL SECTION

Materials and Chemicals. Sulfuric acid (99.999%), isopropyl alcohol, nitric acid (70%), ethylene glycol (anhydrous, 99.8%), acetone, ethanol, Ti foil (thickness 0.127 mm, 99.7%), chloroplatinic acid hydrate (\geq 99.9%), polyvinylpyrrolidone (average MW = 55000), and perfluorinated resin solution containing Nafion 1100W (5 wt % in lower aliphatic alcohols and water, contains 15-20% water) were purchased from Millipore Sigma. Hydrochloric acid was purchased from Millipore. Ruthenium powder (99.9%) was purchased from Strem Chemicals. Ruthenium (5% on activated carbon powder, reduced) was purchased from Alfa Aesar. Nitric acid (TraceMetal grade) was purchased from Fisher Chemical. Metal free grade centrifuge tubes (89049-170) were purchased from VWR. Aluminum chips (99.99%, 1-12 mm) were purchased from Noah Technologies. Flash-dry silver colloidal suspension and glassy carbon plates $(25 \times 25$ × 1 mm) were purchased from SPI Supplies. Poly(vinyl chloride)coated copper wire (UL Style 1007/1569) was purchased from Consolidated Electronic Wire & Cable.

Synthesis of Ru₄Al₁₃ **Single Crystals.** 250 mg of Ru powder and 1250 mg of Al chips were added to a 2 mL cylindrical alumina crucible and heated in an alumina tube under flowing Ar by heating to 1300 °C and holding at that temperature for 10 h. The crucible was then cooled slowly (1 °C/min) to 700 °C, cooled to 300 °C (3 °C/min), and subsequently cooled to room temperature (1 °C/min). The crucible was then broken, and the resulting metal ingot was placed in a solution of 3 M HCl and let sit for 3 days to dissolve the excess Al. The resulting black crystals were separated from the HCl solution via vacuum filtration, washed with deionized, distilled water, and then let dry under ambient conditions. Once dry, the crystals were stored under an Ar atmosphere.

Preparation of Electrodes. Ru_4Al_{13} : A crystal of Ru_4Al_{13} was affixed by using Ag colloidal paint to a poly(vinyl chloride)-coated copper wire that was threaded through a 6 mm diameter glass tube. After drying the Ag paint, all exposed wire and Ag paint were covered with epoxy, leaving only the surface of the Ru₄Al₁₃ crystal exposed. The epoxy was allowed to dry overnight. The geometric surface area of each electrode was determined by analyzing images of the electrode surface obtained with an Epson scanner by using ImageJ software. Ru/ C: An ink of Ru/C was prepared by sonicating 5 mg of Ru/C (5 wt %) in a solution of deionized, distilled H₂O (0.5 mL) and Nafion (20 μ L) for 5 min. A 2.5 × 2.5 cm square glassy carbon plate was wrapped with Teflon tape so that 1.5 cm² of the plate was exposed. 300 μ L of the Ru/C ink was dropcast onto the exposed glassy carbon surface and let dry under ambient conditions. Once dry, the Teflon tape was removed. Pt nanoparticles on Ti foil: Pt nanoparticles were made by using a modified literature procedure. 30 Briefly, a solution of H₂PtCl₆ (96 mg, 0.23 mmol) in ethylene glycol (3 mL) was rapidly injected into a stirring solution of ethylene glycol (21 mL) and PVP (70 mg, MW = 55000) under a blanket of argon at 160 $^{\circ}$ C. The solution was held at this temperature for 10 min and then was let cool to room temperature. The solution was diluted with acetone and centrifuged, followed by the decanting of the resulting supernatant. To wash the resulting particles, the particles were resuspended in ethanol, diluted

with acetone, and centrifuged, followed by the decanting of the supernatant. This washing step was repeated for a total of three times, and the resulting particles were suspended in 4 mL of ethanol. To prepare the electrodes, 20 μ L of this suspension was pipetted onto a 0.55 cm² sheet of Ti foil (loading density \approx 0.23 mg/cm²), and the solvent was allowed to evaporate. To anneal the Pt nanoparticles, the Ti foil was heated in a furnace to 400 °C for 2 h under flowing forming gas. The resulting Pt/Ti foil was then affixed to a poly(vinyl chloride)-coated copper wire that was threaded through a 6 mm diameter glass tube, as described above for the preparation of the Ru₄Al₁₃ electrodes. The geometric surface area of the exposed Pt nanoparticles was obtained by analyzing images of the electrode surface obtained with an Epson scanner using ImageJ software.

Electrochemical Experiments. Unless otherwise stated, electrochemical experiments were performed in a four-necked singlecompartment flask by using 0.5 M H₂SO₄ (99.999%, 150 mL), with a carbon rod counter electrode and a saturated calomel reference electrode (SCE). To establish standard conditions, hydrogen gas was continuously bubbled into the electrolyte solution 30 min prior to and during the electrochemical experiments. The RHE potential was determined from the open circuit potential of a cleaned Pt wire in 0.5 M H₂SO₄. To condition the Ru₄Al₁₃ electrodes, the electrode was held at a current density of -10 mA/cm² for 1 h, based off of the geometric surface area, with the exception of the -100 mA/cm² chronopotentiometry experiment, for which conditioning was performed by holding at a current density of -100 mA/cm² for 1 h. For chronopotentiometry experiments, preconditioned electrodes were held at -10 mA/cm² or -100 mA/cm², based off of geometric surface area, for 24 h, and iR corrections were applied by using the measured uncompensated resistance from each electrode. Polarization data for all electrodes was collected by performing five successive scans of preconditioned electrodes from +0.01 to -0.40 V vs RHE with a sweep rate of 10 mV/s by using the current interrupt method to account for uncompensated resistance. All reported scans are shown from the fifth scan.

Dissolution Studies. Dissolution studies were conducted in a two-compartment cell segregated by a Nafion proton exchange membrane by using 0.5 M H₂SO₄ as the electrolyte, a newly purchased carbon rod as the counter electrode, an SCE reference electrode, and a prepared Ru₄Al₁₃ electrode as the working electrode. The two-compartment cell was utilized for these measurements to prevent any trace Al on the carbon rod from leaching into the analyzed electrolyte in the working component of the cell. A stir bar was allowed to spin slowly in the solution during the entire duration of the experiment to facilitate homogeneous dispersion of dissolved ions in solution. The catalyst was conditioned for 1 h by holding the working electrode at a current density of -10 mA/cm² and then taking aliquots of the solution in the working component of the cell at t = 0, 15, 30, and 45 min. Then, the catalyst was held at a current density of -10 mA/cm^2 for 24 h, and then aliquots were taken from the working component of the cell at t = 0, 2, 6, 12, and 24 h. Each aliquot was stored in trace metal free grade centrifuge tubes and diluted with ultrahigh-purity HNO3 and deionized, distilled H2O, yielding 2.2% HNO₃/0.1% H₂SO₄ solutions that were analyzed via ICP-MS.

Faradaic Efficiency Measurements. Faradaic efficiency measurements were conducted in an airtight two-compartment cell with 0.5 M $\rm H_2SO_4$ (99.999%, 150 mL), equipped with a Nafion membrane, a carbon rod counter electrode, a SCE reference electrode, and a $\rm Ru_4Al_{13}$ working electrode. A tube was run from the cell to an inverted water-filled graduated cylinder submerged in a bath of water. The working electrode was allowed to run at a current density of $-100~\rm mA/cm^2$ ($-4.5~\rm mA$ for the tested electrode) for 1 h to condition the catalyst. To conduct quantitative Faradaic efficiency measurements, the catalyst was run at a current density of $-100~\rm mA/cm^2$ for 2 h, and the volume of air in the inverted graduated cylinder was recorded in 15 min intervals.

Characterization. Powder X-ray diffraction (XRD) data were collected by a Bruker D-8 Advance X-ray diffractometer using Cu $K\alpha$ radiation and a Lynx Eye 1-D detector. About 8–10 single crystals

were ground up into a fine powder by using a mortar and pestle to conduct powder XRD. Simulated XRD patterns were generated with the Crystal Maker/Crystal Diffract software package using published crystallographic data for each phase.³¹ To prepare samples for scanning electron microscopy (SEM) of the crystals, carbon tape (Ted Pella) was applied to the SEM stubs, and single crystals were placed on the tape. To obtain the SEM images of the cross section, a crystal was broken in half and then placed vertically on the stub. SEM images were obtained with a FEI Nova Nano-SEM FESEM at an accelerating voltage of 5 keV and a working distance of 3.5 mm. Energy dispersive spectroscopy (EDS) data and elemental mapping images were collected at an accelerating voltage of 20 keV and a working distance of 5 mm. EDS maps display signals from Ru L α and Al K α peaks. X-ray photoelectron spectra (XPS) were collected on a PHI VersaProbe II spectrometer equipped with a monochromatic Al $K\alpha$ X-ray source ($h\nu$ = 1486.6 eV) and a concentric hemispherical analyzer. Charge neutralization was performed by using low-energy electrons and argon ions for all acquired spectra. Survey and highresolution scans were acquired at pass energies of 117.4 and 29.4 eV, respectively. Samples were electrically isolated and mounted to the platen by using double-sided Scotch tape. Measurements were made at a takeoff angle of 45° with respect to the sample surface plane, which resulted in a typical sampling depth of 3-6 nm. To curve fit the Ru(3d) spectra, reference line shapes were derived from the literature spectra of metallic Ru and hydrated RuO₂ samples.³² These derived line shapes were then used to fit the Ru(3d) experimental spectra. Additionally, a C(1s) component was added into the experimental Ru(3d) region as the energy regions for C(1s) and Ru(3d) overlap. Finally, all peaks were charge-referenced to the C(1s) component at 284.8 eV.

Calculation of Pourbaix Diagrams. Pourbaix diagrams of Ru₄Al₁₃ were calculated by using the computational procedure developed by Persson et al.,³³ as implemented in the pymatgen (Python Materials Genomics) library.³⁴ Energy corrections were applied to the free energy of compounds in an aqueous solution. The corrected reference energies are the following: 1.4 eV/O₂.³⁵ Five sets of concentrations for Ru and Al cations were chosen to build the Pourbaix diagrams in Figure S1. These concentrations correspond to experimentally relevant corrosion conditions obtained from electrochemical measurements. The aqueous stability of Ru₄Al₁₃ with respect to the most stable Pourbaix phase is visualized by the superimposed color map. All of the Pourbaix diagrams were generated at 25 °C.

■ RESULTS AND DISCUSSION

 Ru_4Al_{13} adopts a monoclinic crystal structure that can be described as consisting of both puckered and planar Ru sheets lying in the [010] direction embedded in a three-dimensional Al framework (Figure 1a). Ru_4Al_{13} was synthesized as millimeter-scale crystals by using an aluminum flux. Briefly, Ru powder and Al chips in the Ru:Al molar ratio of 5:95 were heated to 1300 $^{\circ}\text{C}$ for 10 h under flowing Ar, then slowly cooled to 700 $^{\circ}\text{C}$, and then more rapidly cooled to room temperature. The Ru_4Al_{13} crystals, which had typical dimensions of 2 \times 2 \times 0.2 mm, were isolated from the flux by dissolving the excess Al with 3 M HCl.

Extracting single crystals from the fluxes in which they were grown is often achieved by dissolving the flux in acid, as was done here. For crystals that are sensitive to acid-induced corrosion, the flux dissolution process must be performed carefully to avoid roughening the surface or corroding the material. We surmised that if the ultimate goal was actually to roughen the surface, then it would be desirable to dissolve the flux more aggressively and allow the acid to begin attacking the surfaces of the crystals. Accordingly, while millimeter-scale metallic crystals are typically shiny, the Ru₄Al₁₃ crystals isolated from the Al flux appeared as a matte black color (Figure 1b). SEM imaging (Figure 1c) revealed that the surfaces of the

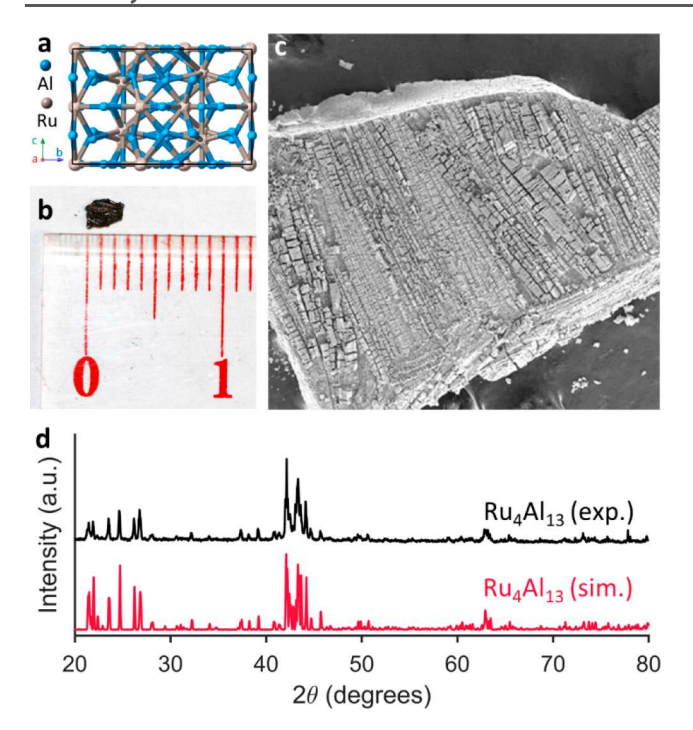


Figure 1. (a) Crystal structure of Ru_4Al_{13} , based on crystallographic data in ref 31. (b) Photograph (with a ruler as a 1 cm scale bar) and (c) SEM image of a Ru_4Al_{13} single crystal. (d) Experimental XRD pattern of a ground single crystal of Ru_4Al_{13} along with a simulated XRD pattern (based on crystallographic data in ref 31) for comparison.

 Ru_4Al_{13} crystals were indeed rough, with pits and trenches etched into them by the acid used to dissolve the Al flux. A portion of the isolated crystals were ground into a powder, and the resulting powder XRD pattern confirmed that they are Ru_4Al_{13} (Figure 1d). The experimental XRD pattern matches well with a simulated XRD pattern that is based on available crystallographic data. An XRD pattern for a collection of Ru_4Al_{13} single crystals from which the powder in Figure 1 was derived is included in Figure S2. The XRD pattern indicates significant preferred orientation from the single crystals, diffracting primarily (h00) and $(h0\overline{1})$ planes

A cross section of a Ru₄Al₁₃ crystal (obtained after breaking the crystal in half, Figure S3) appears smoother than the surface, as seen in the SEM image in Figure 2a. EDS maps of the cross section (Figure 2b,c) indicated the presence of a Ru₄Al₁₃ core in the etched crystal. Ru and Al were colocalized and distributed uniformly throughout the core of the crystal, and the composition of this region was determined by EDS to be approximately 25:75 Ru:Al, which is consistent with the expected stoichiometric ratio of 24:76 for Ru₄Al₁₃ (Table S1). However, while SEM-EDS maps of the Ru₄Al₁₃ surface (Figure 2d-f) also confirm that Ru and Al are colocalized, the Ru signal is significantly stronger than that of Al, suggesting that the surface of the crystal is Ru-rich. Quantitative analysis of the EDS element maps confirms a Ru:Al ratio of approximately 76:24, which is significantly higher than the expected ratio of 24:76 for Ru₄Al₁₃ (Table S1). This indicates that much of the Al near the surface of the crystal was leached during the flux dissolution process. Removing the Ru₄Al₁₃ crystals from the Al flux by using concentrated HCl therefore resulted in the formation of bulk millimeter-scale crystals with a roughened Ru-rich Ru-Al surface and a Ru₄Al₁₃ core, inferred from bulk

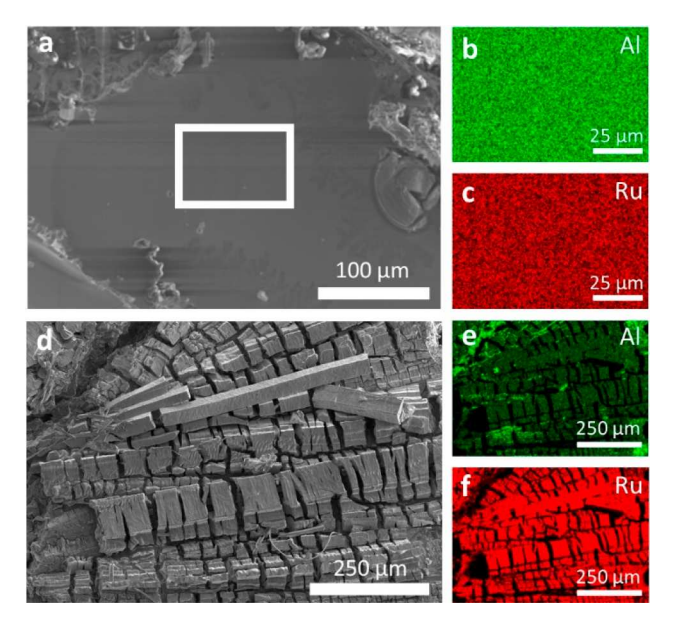


Figure 2. (a) SEM image of a cross section (interior region) of a $\mathrm{Ru_4Al_{13}}$ crystal that was broken in half. The outlined region corresponds to the EDS maps shown to the right, which are for (b) Al and (c) Ru. (d) SEM image of the acid-roughened surface of the $\mathrm{Ru_4Al_{13}}$ crystal along with the corresponding EDS maps for (e) Al and (f) Ru.

XRD analysis of the ground powder and EDS analysis of the cross section.

To determine the catalytic performance of these surfaceroughened crystals for the HER, electrodes were prepared by affixing a millimeter-scale Ru₄Al₁₃ crystal to a poly(vinyl chloride)-coated copper wire by using colloidal Ag paint and covering the exposed wire with epoxy, leaving only the surface of the Ru₄Al₁₃ crystal exposed (Figure S4). Electrochemical experiments for Ru₄Al₁₃ were performed in a four-necked single-compartment flask by using 0.5 M H₂SO₄ with a carbon rod counter electrode, saturated calomel reference electrode (SCE), and Ru₄Al₁₃ working electrode. For the HER, catalytic performance is often evaluated by using polarization curves, in which the overpotential required to reach benchmark current densities is determined by sweeping the applied potential. If these I-V curves deviate from behavior dictated by the Tafel equation,³⁶ this is often indicative of additional surface redox processes, catalyst corrosion, or mass transport issues, which can make interpretation of catalyst performance challenging. Polarization curves for control electrodes yielded results consistent with those found in the literature, 37,38 as Ru/C was able to reach a current density of -10 mA/cm² at an overpotential of 101 mV and glassy carbon exhibited no measurable catalytic activity at the applied potentials (Figure 3a). However, even after catalyst conditioning, slightly irregular current behavior is observed for Ru₄Al₁₃ electrodes, which is expected, given the propensity for Al species to corrode in acidic media.³⁹

To better evaluate the catalytic performance as well as the stability of the Ru_4Al_{13} crystals for catalyzing the HER, chronopotentiometry (CP) scans were run on electrodes at -10 and -100 mA/cm² for 24 h (Figure 3b). To achieve stable applied potentials for these scans, a preconditioning step was required, in which the catalyst was held at a constant, negative current density for 1 h prior to catalyst testing (Figure S5). After conditioning, these single-crystal electrodes

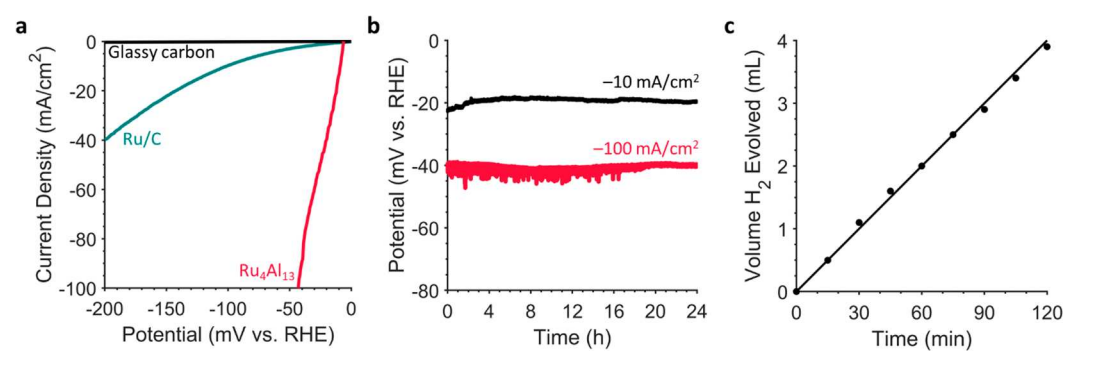


Figure 3. (a) iR-corrected polarization data in 0.5 M H_2SO_4 for a conditioned Ru_4Al_{13} electrode as well as control electrodes for glassy carbon and commercial Ru/C, normalized to geometric surface area. (b) iR-corrected chronopotentiometry data in 0.5 M H_2SO_4 for conditioned Ru_4Al_{13} electrodes, held at -10 and -100 mA/cm² for 24 h. (c) Experimental (circles) and expected (line) volume of evolved hydrogen for a conditioned Ru_4Al_{13} electrode held at -100 mA/cm² for 2 h.

exhibited excellent performance for the HER in 0.5 M H₂SO₄, with the best performing electrodes requiring minimum overpotentials of only 18 and 39 mV to achieve current densities of -10 and -100 mA/cm² (normalized to geometric surface area), respectively. To benchmark these current densities, the catalytic performances of both Pt nanoparticles supported on a Ti electrode and a bulk Pt wire were evaluated (Figures S6 and S7). When normalized to geometric surface area, the performance of Ru₄Al₁₃ was superior to that of a Pt wire and comparable to that of Pt nanoparticles. In addition, these scans demonstrate that the Ru₄Al₁₃ crystals offer significant durability over prolonged use, requiring the same or slightly lower overpotentials to maintain constant H₂ production over the course of 24 h. To evaluate the reproducibility of the scans, a total of four different electrodes, produced both from the same batch as our best performing electrode and from different batches, were run at -10 mA/cm^2 for 24 h (Figure S8). All of these electrodes maintained or increased in catalytic performance over 24 h, with an average lowest applied overpotential of 23.5 \pm 4.8 mV at -10 mA/cm², demonstrating that the high catalytic activity could be reproducibly achieved.

The numerical performance metrics described above are considered to be excellent for a Ru-based HER catalyst in an acidic medium, especially given that the Ru₄Al₁₃ electrodes are bulk materials with roughened surfaces that are estimated to increase the surface area only marginally relative to that of a flat single-crystal surface. The overpotential at $-10~\text{mA/cm}^2$ was better than or comparable to previously reported Ru-based HER catalysts in acid, including commercial Ru/C (69 mV),³⁷ Ru on graphene-like layered carbon (35 mV),³⁷ a porous Ru nanomaterial (83 mV),⁴⁰ and RuP₂ nanoparticles encapsulated by N,P-codoped carbon (38 mV)¹⁰ but slightly worse than Ru nanocrystals on C₂N (13.5 mV).⁸ The high activity of the Ru₄Al₁₃/Ru_xAl_y catalyst is likely attributable to the architecture of the surface of the crystal, including the rough, Ru-enriched surface region. However, additional electronic effects induced by the Al cannot be ruled out.

To help verify that the observed currents for these CP scans were attributed to the HER and not other redox processes, such as catalyst degradation or chemical surface modification, we calculated the Faradaic efficiency (FE) of the Ru_4Al_{13} single crystals for the production of H_2 . A conditioned Ru_4Al_{13} electrode was held at a constant current density of -100 mA/cm², which corresponded to -4.5 mA for this particular electrode, in an airtight electrochemical cell. The evolved H_2

was then collected in an inverted, submerged graduated cylinder. Over 2 h for the conditioned Ru_4Al_{13} electrode, the rate of H_2 production remained constant (Figure 3c), and the collected volume of H_2 (3.9 mL) matched closely with the expected volume evolved for a catalyst with 100% FE (4.0 mL), resulting in an observed FE of 97%. These FE results are consistent with the conditioned Ru_4Al_{13} electrodes catalyzing the HER on the catalyst surface. Note that the electrochemically active surface area (ECSA) could not be calculated because there were no regions without competing electrochemical processes due to Al corrosion.

Knowing that Al is susceptible to dissolution, we sought to investigate the potential corrosion of the catalyst over the course of the CP scans. To do this, aliquots of the electrolyte solution were collected during both the conditioning and catalytic testing stages for a Ru_4Al_{13} electrode held at -10 mA/cm² for 24 h; these aliquots were then analyzed via ICP-MS (Figures 4 and Figure S9). During the conditioning step, a

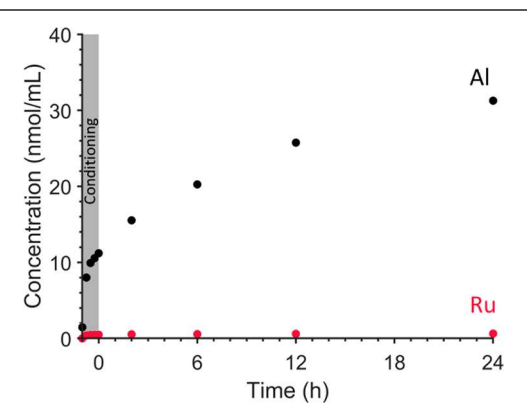


Figure 4. Dissolution data (ICP) for Ru and Al over 24 h for a conditioned Ru_4Al_{13} electrode held at $-10~mA/cm^2$.

rapid rise in the dissolution of both Ru and Al was observed. While no significant additional dissolution of Ru was observed after the conditioning step, Al dissolution continued during the entire CP scan and began to plateau around 24 h. The conditioning step quickly enriches the surface in Ru. The Al that dissolves during the CP scan likely comes from the subsurface region or deeper into the crystal and therefore does not significantly change the surface composition. Over the course of this CP scan, a total of 67.5 μ g of Al (from the ~25 mg crystal) dissolved in solution, which would correspond to

the generation of 3.75 μ mol of H₂. The electrode that was tested had a geometric surface area of 0.044 cm², and the expected total evolved H₂ over 24 h at a current density of -10 mA/cm² was 197 μ mol of H₂. From this result, it can be seen that the amount of H₂ produced from Al dissolution is quite small (<2%) in comparison to the amount of H₂ produced catalytically, confirming that the majority of the H₂ produced was from the HER.

At the end of catalytic testing, the concentration of Al in the electrolyte solution was found to be \sim 50 times that of Ru. This remarkable difference indicates that Al was significantly more prone to leaching into solution than Ru, especially during the conditioning step, despite it being much less abundant on the surface of the catalyst. Because of this, we performed three additional studies. We first used SEM and EDS to analyze the final Ru₄Al₁₃ electrode to determine the morphology and composition of the crystal after testing. We then computationally constructed a Pourbaix diagram to understand the composition evolution during catalysis as a function of pH and applied potential. Finally, we used XPS to determine the surface composition before and after testing.

The morphology and composition of the Ru_4Al_{13} catalyst were microscopically investigated after catalytic testing to determine whether there were any significant changes to the surface relative to before testing. Figure S10 shows SEM-EDS images of the surface of Ru_4Al_{13} after the 24 h CP measurement at $-10~\text{mA/cm}^2$. The morphology and surface roughness did not appear to change post-testing. The composition determined by using EDS confirmed the presence of both Ru and Al on the surface, with the Ru:Al ratio (90:10) being more Ru-rich than the composition of the catalyst surface prior to testing (Ru:Al = 75:25). The slight decrease in Al concentration from the surface region was attributed to its dissolution as Al^{3+} , while Ru remained on the surface and became enriched relative to pretesting.

Figure 5 shows a Ru-Al Pourbaix diagram that was computationally constructed by using an *ab initio* calculated

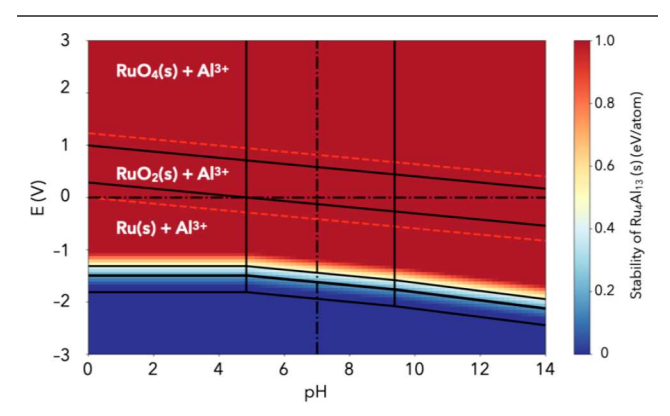


Figure 5. Calculated Pourbaix diagram for Ru_4Al_{13} . The aqueous stability of the Ru_4Al_{13} phase is visualized by the superimposed color map. Phase boundaries (solid black lines), boundaries for the onset of the HER and OER (lower and upper dashed red lines), and regions of neutral pH and potential (dashed black lines) are highlighted.

 Ru_4Al_{13} solid. This diagram suggests that the most stable species present at the pH (0.3) and applied potential (-20 mV) of the CP measurements are Ru(s) and Al^{3+} , which is consistent with what was observed experimentally in the surface region; Al dissolution continued while Ru plateaued and became enriched on the surface. Additional Pourbaix

diagrams were constructed, taking into account the concentrations of Ru and Al observed in the electrolyte solution after 24 h, to factor in boundary shifting that may occur as a result of these increasing ion concentrations in solution. While a small amount of boundary shifting was observed (Figure S1), it did not result in any change to the most thermodynamically stable species that would be present, suggesting that the dissolution behavior seen at the beginning of the CP scan remains consistent throughout; this is consistent with the experimentally observed dissolution data.

To further understand the evolution of the catalyst surface during testing, XPS was used to determine the surface composition both prior to and after CP scans (Figure S11 and Table S2). The Al(2p) region for both untested (Figure 6a) and tested (Figure 6b) Ru₄Al₁₃ crystals indicated the

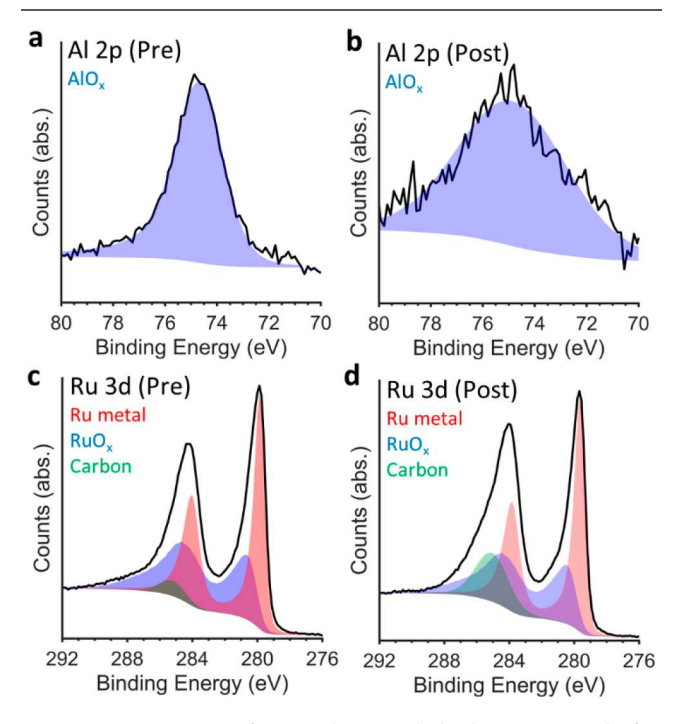


Figure 6. XPS spectra for Ru_4Al_{13} crystals both prior to and after chronopotentiometry scans for both the Al 2p (a, Pre; b, Post) and Ru 3d (c, Pre; d, Post) regions. Curve fittings represent contributions from oxidized (blue) and metallic (red) species as well as the C 1s contribution (green).

presence of only one Al 2p peak, which was centered at 74.6 \pm 0.1 eV. These peak positions correspond well to an oxidized Al species, most likely to be Al₂O₃.⁴¹ The curve fit of the Ru(3d) spectra required consideration of the overlapping energies of the C(1s) and the Ru(3d) regions. A detailed description of the curve fitting process can be found in the Experimental Section. The results of the curve fit to the Ru(3d) region are shown in Figures 6c (untested) and 6d (tested), with detailed fitting data are shown in Figure S12. Two sets of peaks centered at 279.7 and 280.5 eV are observed, and these correspond well with Ru metal and hydrated RuO2, respectively.³² Additionally, the peak corresponding to C(1s) is also noted at the calibrated energy value of 284.8 eV. In the Ru₄Al₁₃ sample prior to testing, the Ru to Al ratio was approximately 44:56, whereas after catalysis, the Ru:Al ratio had increased to approximately 60:40. Concomitant with the decrease in Al(2p) signal, the O(1s) peaks corresponding to an

 AlO_x species (531.8 eV) also decreased in intensity while the peak attributed to a RuO_x species (529.7 eV) remained largely unchanged (Figure S13). The loss of Al from the surface of the Ru_4Al_{13} crystals after catalysis agrees well with the experimental ICP-MS data and the computationally predicted Pourbaix diagrams discussed above. Finally, the large increase in the carbon signal observed in the postcatalysis sample is attributed to the epoxy used to fabricate the electrodes.

CONCLUSIONS

In summary, Ru₄Al₁₃ single crystals with millimeter-scale dimensions evolve, in the presence of strong acid, into a surface-roughened derivative having a Ru-rich Ru-Al surface and a Ru₄Al₁₃ core due to acid leaching of Al. This evolution continues under applied potentials, consistent with a computationally generated Pourbaix diagram, to produce a bulk material that catalyzes the HER in 0.5 M H₂SO₄ with overpotentials at geometrically normalized current densities that are on par with those of Pt, the benchmark catalyst for this reaction. These results establish in situ surface-modified Ru₄Al₁₃ as a highly active HER catalyst in acidic electrolytes and demonstrate that postsynthetic dealloying of bulk intermetallic crystals is a viable method for the development of robust catalysts for the HER. This potentially generalizable pathway could be used to engineer higher surface area analogues of catalytic materials that can only be prepared as bulk-scale crystals.

ASSOCIATED CONTENT

Supporting Information

The Supporting Information is available free of charge at https://pubs.acs.org/doi/10.1021/acs.chemmater.1c02583.

Additional images of the Ru_4Al_{13} crystals and electrodes, electrode conditioning data, XRD data for Pt nanoparticles, polarization and chronopotentiometry data, dissolution data, SEM and EDS data, Pourbaix diagrams, and XPS data (PDF)

AUTHOR INFORMATION

Corresponding Author

Raymond E. Schaak – Department of Chemistry, Materials Research Institute, and Department of Chemical Engineering, The Pennsylvania State University, University Park, Pennsylvania 16802, United States; oorcid.org/0000-0002-7468-8181; Email: res20@psu.edu

Authors

Kriti Seth – Department of Chemistry, The Pennsylvania State University, University Park, Pennsylvania 16802, United States

Albert J. Darling – Department of Chemistry, The Pennsylvania State University, University Park, Pennsylvania 16802, United States

Cameron F. Holder – Department of Chemistry, The Pennsylvania State University, University Park, Pennsylvania 16802, United States; ⊚ orcid.org/0000-0003-1036-4142

Yihuang Xiong — Department of Materials Science and Engineering, The Pennsylvania State University, University Park, Pennsylvania 16802, United States; ⊚ orcid.org/0000-0001-7809-6047

Jeffrey R. Shallenberger – Materials Research Institute, The Pennsylvania State University, University Park, Pennsylvania 16802, United States

Complete contact information is available at: https://pubs.acs.org/10.1021/acs.chemmater.1c02583

Author Contributions

K.S. and A.J.D. contributed equally to this work.

Notes

The authors declare no competing financial interest.

ACKNOWLEDGMENTS

This work was supported by the American Chemical Society Petroleum Research Fund under Grant #58373-ND5. The computational work was supported by the National Science Foundation under Grant DMREF-1729338. Microscopy, diffraction, and XPS data were collected at the Materials Characterization Lab of the Penn State Materials Research Institute. The authors thank Ismaila Dabo for helpful discussions about the Pourbaix diagrams and Lucas Alameda for helpful discussions about synthesis and catalytic testing.

■ REFERENCES

- (1) Lewis, N. S.; Nocera, D. G. Powering the Planet: Chemical Challenges in Solar Energy Utilization. *Proc. Natl. Acad. Sci. U. S. A.* **2006**, 103, 15729–15735.
- (2) United States Department of Energy. A National Vision of America's Transition to a Hydrogen Economy—To 2030 and Beyond; Washington, DC, 2003.
- (3) Zhu, J.; Hu, L.; Zhao, P.; Lee, L. Y. S.; Wong, K.-Y. Recent Advances in Electrocatalytic Hydrogen Evolution Using Nanoparticles. *Chem. Rev.* **2020**, *120*, 851–918.
- (4) Trasatti, S. Work Function, Electronegativity, and Electrochemical Behaviour of Metals: III. Electrolytic Hydrogen Evolution in Acid Solutions. *J. Electroanal. Chem. Interfacial Electrochem.* 1972, 39, 163–184
- (5) Seh, Z. W.; Kibsgaard, J.; Dickens, C. F.; Chorkendorff, I.; Nørskov, J. K.; Jaramillo, T. F. Combining Theory and Experiment in Electrocatalysis: Insights into Materials Design. *Science* **2017**, *355*, 1.
- (6) Bae, S.-Y.; Mahmood, J.; Jeon, I.-Y.; Baek, J.-B. Recent Advances in Ruthenium-Based Electrocatalysts for the Hydrogen Evolution Reaction. *Nanoscale Horiz.* **2020**, *5*, 43–56.
- (7) Ledendecker, M.; Mondschein, J. S.; Kasian, O.; Geiger, S.; Göhl, D.; Schalenbach, M.; Zeradjanin, A.; Cherevko, S.; Schaak, R. E.; Mayrhofer, K. Stability and Activity of Non-Noble-Metal-Based Catalysts Toward the Hydrogen Evolution Reaction. *Angew. Chem., Int. Ed.* **2017**, *56*, 9767–9771.
- (8) Mahmood, J.; Li, F.; Jung, S.-M.; Okyay, M. S.; Ahmad, I.; Kim, S.-J.; Park, N.; Jeong, H. Y.; Baek, J.-B. An Efficient and pH-Universal Ruthenium-Based Catalyst for the Hydrogen Evolution Reaction. *Nat. Nanotechnol.* **2017**, *12*, 441–446.
- (9) Li, F.; Han, G.-F.; Noh, H.-J.; Ahmad, I.; Jeon, I.-Y.; Baek, J.-B. Mechanochemically Assisted Synthesis of a Ru Catalyst for Hydrogen Evolution with Performance Superior to Pt in Both Acidic and Alkaline Media. *Adv. Mater.* **2018**, *30*, 1803676.
- (10) Pu, Z.; Amiinu, I. S.; Kou, Z.; Li, W.; Mu, S. RuP₂-Based Catalysts with Platinum-like Activity and Higher Durability for the Hydrogen Evolution Reaction at All pH Values. *Angew. Chem., Int. Ed.* **2017**, *56*, 11559–11564.
- (11) Liu, Y.; Liu, S.; Wang, Y.; Zhang, Q.; Gu, L.; Zhao, S.; Xu, D.; Li, Y.; Bao, J.; Dai, Z. Ru Modulation Effects in the Synthesis of Unique Rod-like Ni@Ni₂P—Ru Heterostructures and Their Remarkable Electrocatalytic Hydrogen Evolution Performance. *J. Am. Chem. Soc.* 2018, 140, 2731–2734.
- (12) Axet, M. R.; Philippot, K. Catalysis with Colloidal Ruthenium Nanoparticles. *Chem. Rev.* **2020**, *120*, 1085–1145.

- (13) Yin, A.-X.; Liu, W.-C.; Ke, J.; Zhu, W.; Gu, J.; Zhang, Y.-W.; Yan, C.-H. Ru Nanocrystals with Shape-Dependent Surface-Enhanced Raman Spectra and Catalytic Properties: Controlled Synthesis and DFT Calculations. J. Am. Chem. Soc. 2012, 134, 20479—20489.
- (14) Murray, R. Method of Producing Finely-Divided Nickel. US 1628190A, May 10, 1927.
- (15) Pavlic, A. A.; Adkins, H. Preparation of a Raney Nickel Catalyst. *J. Am. Chem. Soc.* **1946**, *68*, 1471–1471.
- (16) Rayhan, U.; Kowser, Z.; Islam, M. N.; Redshaw, C.; Yamato, T. A Review on the Recent Advances in the Reductions of Carbon—Carbon/Oxygen Multiple Bonds Including Aromatic Rings Using Raney Ni—Al Alloy or Al Powder in the Presence of Noble Metal Catalysts in Water. *Top. Catal.* **2018**, *61*, 560–574.
- (17) Birry, L.; Lasia, A. Studies of the Hydrogen Evolution Reaction on Raney Nickel-Molybdenum Electrodes. *J. Appl. Electrochem.* **2004**, 34, 735–749.
- (18) Bates, M. K.; Jia, Q.; Doan, H.; Liang, W.; Mukerjee, S. Charge-Transfer Effects in Ni-Fe and Ni-Fe-Co Mixed-Metal Oxides for the Alkaline Oxygen Evolution Reaction. ACS Catal. 2016, 6, 155–161.
- (19) Alameda, L. T.; Holder, C. F.; Fenton, J. L.; Schaak, R. E. Partial Etching of Al from MoAlB Single Crystals To Expose Catalytically Active Basal Planes for the Hydrogen Evolution Reaction. *Chem. Mater.* **2017**, *29*, 8953–8957.
- (20) Urabe, K.; Yoshioka, T.; Ozaki, A. Ammonia Synthesis Activity of a Raney Ruthenium Catalyst. *J. Catal.* **1978**, *54*, 52–56.
- (21) Takeishi, K.; Aika, K.-I. Study of Raney Ruthenium Catalyst for Methanol Synthesis. *J. Catal.* **1992**, *136*, 252–257.
- (22) Hikita, T.; Aika, K.; Onishi, T. Alkali Nitrate Promoted Raney Ru Catalyst as a Superior Catalyst for Ammonia Synthesis. *Catal. Lett.* **1990**, *4*, 157–161.
- (23) Yano, T.; Ogata, Y.; Aika, K.; Onishi, T. Selective Formation of Methanol over Water-Treated Raney Ruthenium. *Chem. Lett.* **1986**, 15, 303–306.
- (24) Semiz, L.; Abdullayeva, N.; Sankir, M. Nanoporous Pt and Ru Catalysts by Chemical Dealloying of Pt-Al and Ru-Al Alloys for Ultrafast Hydrogen Generation. *J. Alloys Compd.* **2018**, 744, 110–115.
- (25) Semiz, L. Dehydrogenation of Ammonia Borane by Dealloyed Ruthenium Catalysts. *Inorg. Nano-Met. Chem.* **2021**, *51*, 20–26.
- (26) Piccolo, L.; Chatelier, C.; De Weerd, M.-C.; Morfin, F.; Ledieu, J.; Fournée, V.; Gille, P.; Gaudry, E. Catalytic Properties of Al₁₃TM₄ Complex Intermetallics: Influence of the Transition Metal and the Surface Orientation on Butadiene Hydrogenation. *Sci. Technol. Adv. Mater.* **2019**, 20, 557–567.
- (27) Armbrüster, M.; Kovnir, K.; Friedrich, M.; Teschner, D.; Wowsnick, G.; Hahne, M.; Gille, P.; Szentmiklósi, L.; Feuerbacher, M.; Heggen, M.; Girgsdies, F.; Rosenthal, D.; Schlögl, R.; Grin, Y. Al₁₃Fe₄ as a Low-Cost Alternative for Palladium in Heterogeneous Hydrogenation. *Nat. Mater.* **2012**, *11*, 690–693.
- (28) Armbrüster, M.; Kovnir, K.; Grin, J.; Schlogl, R.; Gille, P.; Heggen, M.; Feuerbacher, M. Ordered Cobalt-Aluminum and Iron-Aluminum Intermetallic Compounds as Hydrogenation Catalysts. US8822746B2, October 20, 2010.
- (29) Zhang, H.; Liu, Q.; Xu, J.; Wei, L.; Liu, Q.; Kong, X. Holey Ruthenium Nanosheets with Moderate Aluminum Modulation toward Hydrogen Evolution. *Inorg. Chem.* **2019**, *58*, 8267–8270.
- (30) Herricks, T.; Chen, J.; Xia, Y. Polyol Synthesis of Platinum Nanoparticles: Control of Morphology with Sodium Nitrate. *Nano Lett.* **2004**, *4*, 2367–2371.
- (31) Villars, P. Pearson's Handbook: Desk ed.: Crystallographic Data for Intermetallic Phases; ASM International: 1997.
- (32) Morgan, D. J. Resolving Ruthenium: XPS Studies of Common Ruthenium Materials. Surf. Interface Anal. 2015, 47, 1072–1033.
- (33) Persson, K. A.; Waldwick, B.; Lazic, P.; Ceder, G. Prediction of Solid-Aqueous Equilibria: Scheme to Combine First-Principles Calculations of Solids with Experimental Aqueous States. *Phys. Rev. B: Condens. Matter Mater. Phys.* **2012**, *85*, 235438.
- (34) Ong, S. P.; Richards, W. D.; Jain, A.; Hautier, G.; Kocher, M.; Cholia, S.; Gunter, D.; Chevrier, V. L.; Persson, K. A.; Ceder, G. Python Materials Genomics (Pymatgen): A Robust, Open-Source

- Python Library for Materials Analysis. Comput. Mater. Sci. 2013, 68, 314-319.
- (35) Perdew, J. P.; Burke, K.; Ernzerhof, M. Generalized Gradient Approximation Made Simple. *Phys. Rev. Lett.* **1996**, 77, 3865–3868.
- (36) Bard, A.; Faulkner, L. Electrochemical Methods: Fundamentals and Applications, 2nd ed.; John Wiley & Sons: 2000.
- (37) Chen, Z.; Lu, J.; Ai, Y.; Ji, Y.; Adschiri, T.; Wan, L. Ruthenium/ Graphene-like Layered Carbon Composite as an Efficient Hydrogen Evolution Reaction Electrocatalyst. *ACS Appl. Mater. Interfaces* **2016**, 8, 35132–35137.
- (38) Yang, J.; Chen, B.; Liu, X.; Liu, W.; Li, Z.; Dong, J.; Chen, W.; Yan, W.; Yao, T.; Duan, X.; Wu, Y.; Li, Y. Efficient and Robust Hydrogen Evolution: Phosphorus Nitride Imide Nanotubes as Supports for Anchoring Single Ruthenium Sites. *Angew. Chem.* **2018**, *130*, 9639–9644.
- (39) Roberge, P. R. Corrosion Engineering: Principles and Practice; McGraw-Hill: 2008.
- (40) Drouet, S.; Creus, J.; Collière, V.; Amiens, C.; García-Antón, J.; Sala, X.; Philippot, K. A Porous Ru Nanomaterial as an Efficient Electrocatalyst for the Hydrogen Evolution Reaction Under Acidic and Neutral Conditions. *Chem. Commun.* **2017**, *53*, 11713–11716.
- (41) Strohmeier, B. R. An ESCA Method for Determining the Oxide Thickness on Aluminum Alloys. *Surf. Interface Anal.* **1990**, *15*, 51–56.